Uniaxial magnetic anisotropy of cobalt films deposited on sputtered MgO(001) substrates

Kai Chen,[1,3,*] Robert Frömter,[1] Stefan Rössler,[1] Nikolai Mikuszeit,[2] and Hans Peter Oepen[1]

[1]*Institut für Angewandte Physik, Universität Hamburg, Jungiusstr. 11, 20355 Hamburg, Germany*

[2]*Instituto Madrileño de Estudios Avanzados en Nanociencia, IMDEA-Nanociencia, Campus Universidad Autónoma de Madrid, 28049 Madrid, Spain*

[3]*Institute for Materials Research, Helmholtz-Zentrum Geesthacht, 21502 Geesthacht, Germany*

(Received 26 April 2012; revised manuscript received 4 July 2012; published 22 August 2012; publisher error corrected 24 August 2012)

We present a systematic investigation of the in-plane uniaxial magnetic anisotropy induced by the morphology due to ion erosion of MgO(001). Ion milling at oblique incidence forms a ripple structure on the MgO surface the grooves run along the ion beam direction. Ultrathin cobalt films grown on such templates show a dominant uniaxial magnetic anisotropy with the easy axis along the ion beam direction. Both the strength of anisotropy and its symmetry can be controlled via the milling conditions, allowing one to fine-tailor the anisotropy in magnetic films. A uniaxial, volumelike anisotropy contribution is found, which is explained by the modulation of the magnetization perpendicular to the ripples that causes an increase of exchange energy.

DOI: 10.1103/PhysRevB.86.064432 PACS number(s): 75.70.−i, 75.30.Gw, 75.60.Ej, 81.16.−c

I. INTRODUCTION

The artificial tuning of magnetic properties of ultrathin films by means of the surface and interface structure is a fascinating issue from both fundamental and technological points of view.[1–3] In particular, manipulating the magnetic anisotropy is one of the most effective ways to optimize the performance of thin-film based devices.[4–7] Zhan *et al*. demonstrated the capability of tuning of the in-plane uniaxial anisotropy of Fe/MgO(001) films via ion milling.[8] Bisio *et al*. investigated the possibility of isolating the step-induced in-plane uniaxial magnetic anisotropy in order to rule out some ambiguities of vicinal surfaces using an ion sculpted Ag substrate.[9] With respect to applications, it is most advantageous to tailor both the magnitude and symmetry of the magnetic anisotropy.

Changing the morphology of surfaces by oblique-incidence ion beam irradiation has been successfully performed with metals, semiconductors, and insulators.[10–14] Via oblique-incidence ion beam milling, a self-assembled formation of nanometer-scale surface ripples has been observed, which were aligned either parallel or perpendicular to the direction of the ion beam.[15–18] Magnetic films that are deposited on substrates with such microstructure reveal a uniaxial magnetic anisotropy with the easy axis in general along the direction of the ripples.[19–22] Furthermore, the magnitude of the uniaxial magnetic anisotropy can be controlled via the surface morphology, which depends sensitively on the sputtering conditions. Even when a magnetic film is ion milled after deposition, a uniaxial magnetic anisotropy was found due to the formation of ripple structures in the film itself.[7,9,23,24]

In this paper, we report on the manipulation of the uniaxial magnetic anisotropy of ultrathin Co films deposited on MgO(001) that are sputtered by Ar^+ ions prior to the Co deposition. Changing the sputter geometry from normal to oblique incidence (angle of 60° with respect to the surface normal) a transformation from biaxial to uniaxial anisotropy is found for the Co films. It is shown that the anisotropy can be tuned by changing the ion dose Ψ_c. On variation of the film thickness we find a constant anisotropy contribution K_u^v, which we attribute to the volume, and a surface contribution of K_u^s/t, which is inversely proportional to the film thickness.

II. EXPERIMENT

The preparation and characterization of the Co/MgO(001) system is performed in an ultrahigh-vacuum chamber with a base pressure in the low 10^{-7} Pa range, which increases to 1×10^{-6} Pa during Co deposition. The *in situ* magnetic characterization is performed by means of magneto-optic Kerr effect (MOKE). The single-crystal MgO(001) substrate is sputtered with Ar^+ ions at an energy of 1400 eV at room temperature. The sputtering is either performed at normal incidence or at a fixed angle of 60° with respect to the surface normal. After sputtering the substrate is annealed at 800 K for 10 min. This procedure creates a ripple structure on the MgO(001) surface. An atomic force microscopy (AFM) image is shown in Fig. 1(a). A period of ∼100 nm and a height modulation of ∼20 nm (peak-to-peak) is found here for an ion dose of 2.28×10^{17} ions/cm^2, which corresponds to 200 MLE (fcc monolayer equivalent). The ripple structure on the MgO(001) surface is confirmed with *in situ* low-energy electron diffraction (LEED). For sputtering at normal incidence the LEED pattern exhibits a fourfold symmetry [Fig. 1(c)], and it reveals that the fourfold symmetry is not broken upon normal incidence sputtering. Sputtering under grazing incidence, however, creates spots that present an elliptical shape [Figs. 1(d) and 1(e)]. This change of the diffraction pattern originates from a ripple structure with twofold symmetry. In the grazing-incidence geometry the azimuthal orientation of the sample has been varied. In case the in-plane orientation of the beam is changed from parallel to MgO[100] [Fig. 1(d)] to MgO[010] [Fig. 2(e)] the orientation of the long axis of the elliptical spots switches by 90°. The ripples are oriented parallel to the in-plane projection of the ion beam. AFM images were also taken after depositing Co films. For a 10 nm Co film on a rippled MgO surface the AFM image [Fig. 1(f)] reveals that the morphology is preserved in the film. A period of ∼100 nm and a modulation of ∼12 nm (peak-to-peak) is observed.

Co films up to a thickness of 15 monolayers (ML) are deposited by electron-beam evaporation at room temperature. The deposition rate is kept constant at about 2 ML per minute. The film thickness is calibrated using Auger Electron

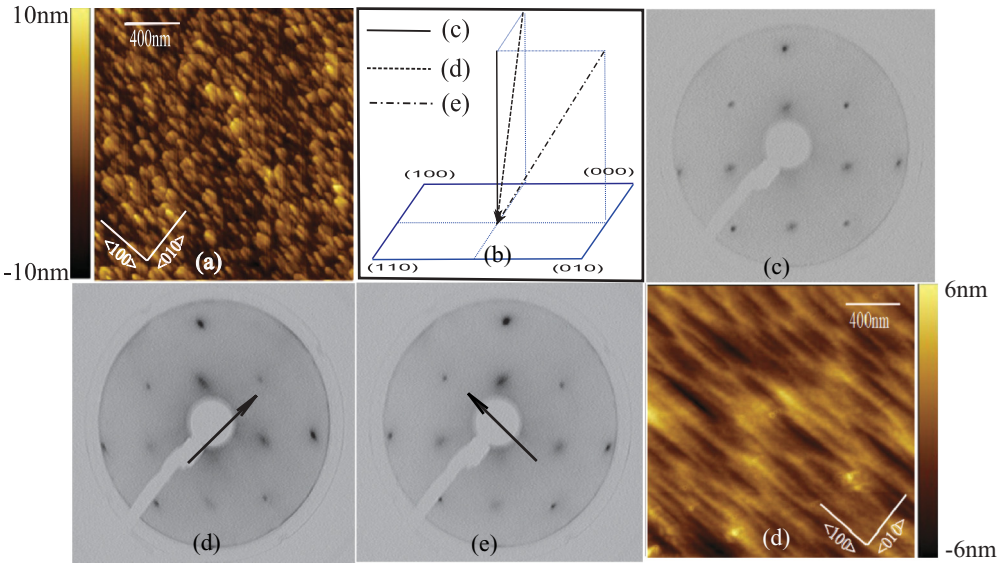

FIG. 1. (Color online) Structure properties of ion milled MgO(001) surfaces. (a) AFM image of a MgO(001) surface with ripple structures after ion milling along MgO[100]; (b) sketch of the ion milling geometry of the different experimental conditions. LEED pattern taken at 220 eV for MgO(001) after (c) normal incidence sputtering, at 60° with respect to the surface normal along (d) MgO[100] and (e) MgO[010] at room temperature. (f) AFM image of a 10 nm Co film deposited on a MgO surface with ripple structure.

Spectroscopy (AES). On a substrate that was sputtered in normal incidence the Co films grow in an fcc structure exhibiting three-dimensional growth, with the Co⟨100⟩—parallel to MgO⟨100⟩ axes. At a thickness of 5.5 ML the films become ferromagnetic at room temperature; more details on the initial growth of Co on MgO can be found in Ref. 25.

III. MAGNETIC PROPERTIES

The films grown on MgO(001) surfaces that were sputtered under normal incidence exhibit a biaxial magnetic anisotropy with easy axes along Co⟨110⟩ [Fig. 2(a)]. The films exhibit uniaxial magnetic behavior when deposited on a MgO(001) that was sputtered at oblique incidence. Figure 2 displays the hysteresis curves obtained for a 9 ML thick film deposited on a MgO(001) sputtered under normal/oblique incidence with doses corresponding to 200 MLE. The in-plane projection of the ion beam was along the [100] direction of the substrate, which causes this axis to become the easy axis of magnetization [Fig. 2(c)]. The same behavior is found when the in-plane orientation of the incoming beam is varied from along MgO[100], to MgO[110], and MgO[010], respectively. In all cases, the MOKE hysteresis curves show very high squareness along and almost no hysteresis perpendicular to the ion beam direction, similar to Fig. 2(c). The angle dependence of the magnetization in remanence normalized to the value in saturation M_r/M_s is plotted in Figs. 2(b) and 2(d). It is evident that a fourfold symmetry is obtained for the substrate sputtered under normal incidence [see the red guideline for the eye in Fig. 2(b)] while for the surfaces with ripples a twofold symmetry is observed [Fig. 2(d)]. The experimental data for the uniaxial films are fitted by a $|\cos\theta|$ function with θ as the in-plane angle of M to the projection of the ion beam direction. The remanence behavior of an ideal fourfold system has the form $\max(|\sin\theta|,|\cos\theta|)$, which has a local minimum depth of $1/\sqrt{2}$. This is not exactly the case in Fig. 2(b) where the minimum is 0.6. Hence it seems that the film decays into domains in remanence when coming from saturation. The results above confirm that the symmetry and the orientation of the uniaxial magnetic behavior can be tuned via the preparation of the substrates by ion milling under oblique incidence.

Next we discuss the thickness dependence of the magnetic behavior. Co films with thicknesses from 5.8 ML, i.e., slightly above the onset of ferromagnetism at room temperature, to 15 ML were grown on MgO(001) milled along the Co[100] in-plane direction under the same conditions as mentioned above. For all thicknesses a dominant uniaxial magnetic anisotropy with the easy axis along MgO[100] is found. The magnetic anisotropy of this system can be described by fourfold (K_c) and uniaxial (K_u) anisotropy contributions, which enter the expression for the free-energy density with in-plane orientation of the magnetization M,

$$E = \frac{K_c}{4}\sin^2 2\theta + K_u \sin^2\theta - M_s H\cos(\phi-\theta), \qquad (1)$$

where θ and ϕ are the angles of the magnetization M and external field H to the uniaxial easy axis, respectively. For all Co films we find that the uniaxial magnetic anisotropy is so large that the fourfold term (K_c) becomes negligible [see Fig. 2(d)]. From hard-axis loops we can determine the uniaxial anisotropy using the slope at small fields. The values of K_u that are extracted from the experimental data are displayed as a function of film thickness in Fig. 3(a). The value of K_u increases with Co thickness. Co films with thickness of 5.85 ML (onset of ferromagnetism) exhibit the lowest value of $K_u = 0.90 \pm 0.20 \times 10^4$ J/m^3, while at a thickness of 13.5 ML the anisotropy constant apparently levels into a maximum value of $K_u = 1.60 \pm 0.30 \times 10^4$ J/m^3. To describe the uniaxial magnetic anisotropy as a function of the thickness (t) of the ferromagnetic layer, we assume

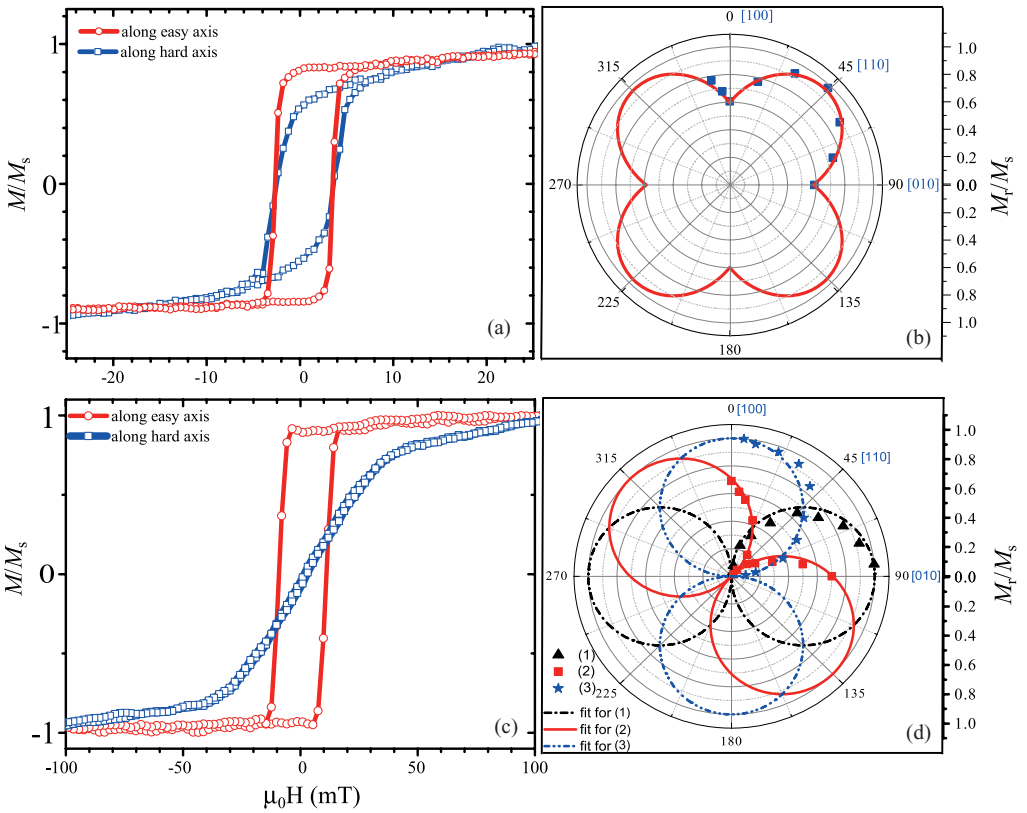

FIG. 2. (Color online) Longitudinal MOKE measurement with the external magnetic field H along the easy and hard axes for 9 ML Co film on MgO(001) surface with (a) flat surface and (c) ripple structure. (b) A polar plot of the remanence as a function of the angle between H and MgO[100] for Co on fourfold surface, and (d) polar plots as a function of the angle of H to the easy axes of the Co film grown on a surface with ripple structure along MgO[100], MgO[110], and MgO[010], respectively.

contributions of both volume (K_u^v) and interfaces (K_u^s) to the anisotropy,

$$K_u = K_u^v + \frac{K_u^s}{t}. \quad (2)$$

Plotting $K_u \times t$ versus Co thickness [Fig. 3(b)] reveals a linear dependence, which proves that the separation into volume and surface contributions is appropriate. The volume contribution K_u^v can be derived from the slope while the interface contribution K_u^s is given by the intercept with the ordinate. From the plot of the data we obtain a volume contribution $K_u^v = 2.15 \times 10^4$ J/m^3 and an interface contribution $K_u^s = -1.45 \times 10^{-5}$ J/m^2. In contrast to results for ion beam sputtered Co/Cu(001)—and Fe/Ag(001) films,[5,7,9,24] additionally to the surface anisotropy a volume contribution to the uniaxial magnetic anisotropy is found. It is interesting to note that the different signs of the two contributions mean that they favor two different in-plane directions. While the volume contribution prefers the alignment of magnetization parallel to the ripple directions, the surface contribution favors the direction perpendicular to the ripples. Two competing contributions can cause a thickness-driven spin reorientation transition. This in-plane reorientation should appear for films of thickness slightly above three monolayers [see zero crossing in inset of Fig. 3(b)], which is far below the onset of ferromagnetism at room temperature (see Ref. 25). A check of this hypothesis at lower temperatures was not made.

To further investigate the dependence of the uniaxial magnetic anisotropy of the Co film on the ion milling conditions, different ion doses of 25, 50, 100, and 200 MLE under otherwise identical conditions were applied under oblique incidence. Films of constant Co thickness (9 ML) were used. The magnetization behavior along and perpendicular to the ripples are investigated via MOKE (Fig. 4). For the smallest ion dose a weak but observable difference can be resolved between the M-H hysteresis loops along the two directions indicating the formation of uniaxial magnetic anisotropy. With increasing ion dose, the magnitude of the uniaxial magnetic anisotropy increases. The hysteresis loops along the hard direction become more and more s-like. Finally, for the highest applied dose a reversible behavior in the hard axis loop appears. The uniaxial anisotropy constant for the last sample is $K_u = 1.5 \pm 0.3 \times 10^4$ J/m^3.

IV. DISCUSSION

At first glance one is led to assume magnetostatic interaction (shape) to be responsible for the uniaxial anisotropy [Fig. 5(a)]. Theoretical models indicating such a relation can be found in literature.[26,27] While in the easiest approach the magnetization is taken as homogeneous within the film[26] the model by Arias and Mills is more accurate in the sense that they consider the locally varying magnetization due to surface morphology. In their theory the exchange contribution

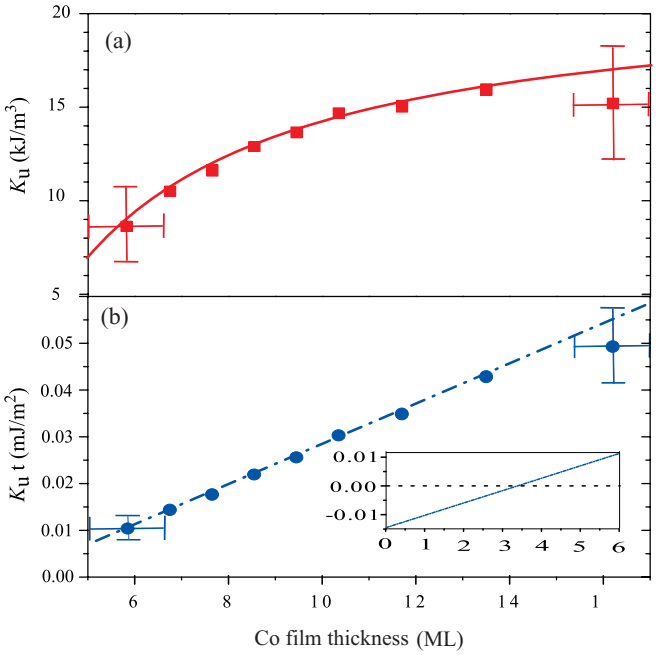

FIG. 3. (Color online) Uniaxial magnetic anisotropy for Co films deposited on MgO(001) surface with ripple structure. (a) K_u versus Co film thickness. (b) $K_u \times t$ plot versus Co film thickness. The lines are fits to the experimental data using Eq. (2). The inset shows the linear extrapolation to smaller thicknesses.

due to the locally varying magnetization orientation is enclosed,[27] however, only the case where the corrugation is small compared to the thickness is worked out. Both theories predict qualitatively the same, namely a surface anisotropy that favors an easy axis of magnetization along the ripples and no bulk contribution. Hence the magnetostatic energy (shape) due to surface charges can be ruled out as an origin for our findings. We have calculated the magnetostatic energy for the

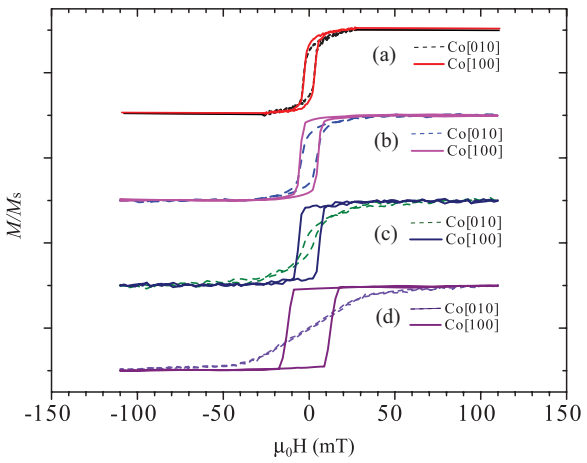

FIG. 4. (Color online) Longitudinal MOKE hysteresis loops for Co films grown on MgO(001) surfaces which were bombarded by different ion doses. The different doses are (a) 25, (b) 50, (c) 100, and (d) 200 MLE. The magnetic field was aligned along and perpendicular to the ion beam direction [100]. The magnitude of the uniaxial magnetic anisotropy increases with the increasing ion dose.

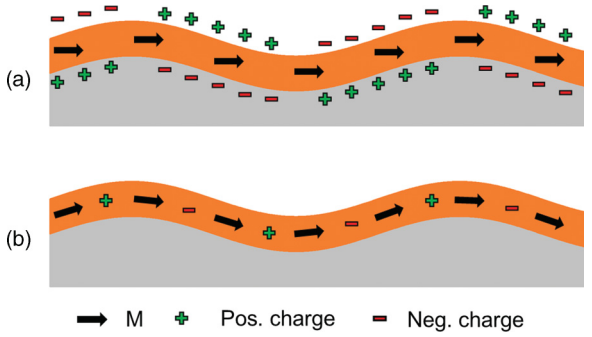

FIG. 5. (Color online) Sketch of two possible magnetic configurations for the magnetization oriented perpendicular to the ripples. (a) When the magnetization orientation in the film (orange) is parallel to the macroscopic film plane surface charges are created due to the corrugation of the mesoscopic surface of the film. Positive charges represent north poles, i.e., sources of magnetic field. (b) When the magnetization follows the rippled structure, surface charges are prevented. In this situation the magnetization deviates slightly from adjacent parts of the film which causes energy contributions due to exchange and volume charges.

situation sketched in Fig. 5(a), i.e., surface charges when the magnetization is parallel to the macroscopic surface (for more details, see the Appendixes). The result for 100 nm periodicity and total ripple heights of 20 nm is plotted in Fig. 6. The $1/t$ behavior of a surface anisotropy is evident with strong contributions at small thicknesses.

Thus the question remains why a volume contribution is found that prefers the easy axis of magnetization along the

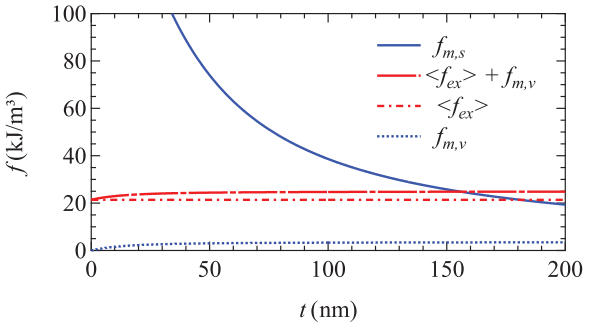

FIG. 6. (Color online) Thickness dependence of the two generic cases of magnetization orientation in films deposited on rippled surfaces. The energy contributions for the two possible configurations shown in Fig. 5 of the magnetization orientation perpendicular to the ripples are shown. Parameters of the surface modulation are as follows: amplitude $h = 10$ nm and wavelength $\lambda = 100$ nm. The magnetic surface charges [see Fig. 5(a)] cause a thickness dependent dipolar energy $f_{(m,s)}$. The $1/t$ dependence [Eq. (B9)] is archetypical for a surface anisotropy. The energy of the configuration shown in Fig. 5(b) is governed by exchange energy $\langle f_{ex} \rangle$ [Eq. (A8)] with a small contribution of dipolar energy caused by volume charges $f_{(m,v)}$ [Eq. (B10)]. The exchange energy has no thickness dependence and corresponds to a bulk anisotropy contribution. The dipolar energy due to volume charges drops off at small thicknesses due to the decrease of total charge. For the films investigated (<4 nm) the total energy of the latter configuration is about one order of magnitude smaller. Further details can be found in the Appendixes.

ripples. Recently, it was found that for the case of Co films epitaxially grown on a vicinal Cu (100) the magnetization shows a thickness dependent tilting out of the mesoscopic surface plane. This tilting appears only when the magnetization is turned into a direction perpendicular to the step edges (in-plane).[28] In the limit of ultrathin films the magnetization was tilted strongest and within the resolution of the experiment found to be parallel to the terrace plane of Cu(1 1 13). The tilting angle (against the macroscopic plane) decreases on thickness increase and the magnetization tends to align with the macroscopic surface plane in the limit of very thick films. The reason for the tilting is the strain of the Co films due to the mismatch of Co to the Cu lattice. In epitaxial films of Co on Cu(001) the tensile strain causes a strong magnetoelastic anisotropy contribution, which supports the shape-induced surface easy plane behavior. In the case of the vicinal surface this means that the magnetoelastic anisotropy contribution favors an orientation of the magnetization within the plane of the terraces. When the magnetization is forced in the direction perpendicular to the step edges, magnetostatic energy contributions appear due to the poles at the terrace edges. This magnetostatic energy is competing with the magnetoelastic effect. As the magnetoelastic contribution to the anisotropy energy is high in the epitaxial system Co/Cu(100), i.e., about 50% of the shape anisotropy (taking a tensile strain of 1.8% in the film plane and magnetoelastic constants of $B_1 = -1.6 \times 10^7$ J/m^3 and $B_2 = +2.6 \times 10^7$ J/m^3 extrapolated from Ref. 29) the magnetostatic energy due to poles at the step edges is of the same order of magnitude only in thick films. Hence to get competing energies the thickness has to be very high (several nm) in Co/Cu(1 1 13). Additionally, there is strain release such that magnetostatics increases while magnetostriction decreases with thickness. In the system Co on sputtered MgO the films show a three-dimensional growth which can reduce strain if present. Thus it can be assumed on firm grounds that the counterpart that forces the magnetization in directions of microfacets is missing in our system. As a consequence the magnetostatic energy is efficient from the very beginning of Co growth on sputtered MgO and the magnetization will align with the macroscopic film plane even in the thin film limit. It is more precise to speak of mesoscopic surfaces here, as on the macroscopic scale the template reveals the ripple structure.

When the magnetization follows the mesoscopic film plane perpendicular to the ripples, the magnetic moments will make small angles with each other while in the direction along the ripples they are aligned perfectly linear. This fact will cause a different exchange energy along and perpendicular to the ripples. This geometry-induced anisotropy can be calculated assuming a simple model for the morphology, i.e., a sinusoidal surface corrugation,

$$h_s(x) = h \sin\left(2\pi \frac{x}{\lambda}\right), \tag{3}$$

with h the amplitude and λ the wavelength of the ripple structure. The exchange energy density for the nonhomogeneous profile is

$$\langle f_{ex} \rangle = \frac{1}{\lambda} \int_0^{\lambda} A \left(\frac{\partial \theta}{\partial x}\right)^2 \mathrm{d}x, \tag{4}$$

with A the exchange stiffness and $\theta(x)$ the position dependent angle of the moments. One obtains in the limit of long wavelength (small slopes) (see the Appendixes)

$$\langle f_{ex} \rangle = \frac{A}{2} \left(\frac{2\pi}{\lambda}\right)^2 \left(\frac{2\pi h}{\lambda}\right)^2. \tag{5}$$

In the Appendixes an explicit expression for the exchange energy at arbitrary large angles is derived. It is used to calculate the energy density for Co on MgO. The result as a function of Co thickness for a period of 100 nm and a modulation of 20 nm (peak-to-peak) is plotted in Fig. 6. As can be seen from the sketch [Fig. 5(b)] additional volume charges are created when the magnetization follows the mesoscopic surface contour. The energy due to the charges is also calculated for the same morphology (for further details see Appendixes) and added to Fig. 6. The magnetostatic energy due to the volume charges is small compared to the exchange-caused energy and gives only a minor correction. Comparing all three energy contributions in the plot it is evident that the sum of energies caused by exchange and volume charges is much smaller than the energy that comes along with surface charges. This proves that the configuration sketched in Fig. 5(b) (magnetization following the mesoscopic surface contour) has a lower energy than the configuration sketched in Fig. 5(a). Hence the lowest state is when the magnetization follows locally the surface morphology and the in-plane anisotropy is given by this magnetization configuration. The results are 8.5 and 21.4×10^3 J/m^3 for the two modulation amplitudes found (6 and 10 nm, respectively). The calculated values are in good agreement with the anisotropy results from the experiment. Hence we may conclude that the proposed exchange-caused anisotropy is a reasonable ansatz to explain the volumelike anisotropy contribution. For the experimentally observed surface contribution that favors the direction perpendicular to the ripples we do not have any reasonable explanation at present.

V. SUMMARY

In summary, we have shown that ion beam sputtering of MgO(001) yields a modification of the surface morphology by forming ripples, which induce a uniaxial magnetic anisotropy in ultrathin ferromagnetic Co films. Varying the film thickness, we have been able to determine the strength of anisotropy and to separate the different uniaxial contributions. In contrast to published results for direct sputtering of ferromagnetic films we find a dominant volume contribution, which we can describe in a simplified model assuming that the magnetization follows the morphology of the mesoscopic surface. The magnetic anisotropy is in the latter case caused by higher exchange energy for magnetization perpendicular to the ripples compared to the direction parallel to the stripes. The importance of the presented results lies in the potential of artificially tuning the properties of magnetic thin films for application.

ACKNOWLEDGMENTS

Thanks go to M. Bubek and A. Neumann for useful discussions. Financial support from DFG via SFB 668 is

acknowledged. H.P.O. wants to acknowledge hospitality at CIC nanoGUNE during his research stay. He is thankful to Basque foundation of Science for the financial support via an Ikerbasque visiting fellowship. N.M. acknowledges funding by Consolider-Ingenio en Nanociencia Molecular ref. CSD200700010, by the Comunidad de Madrid through Project No. S2009/MAT-1726.

APPENDIX A: EXCHANGE ENERGY [SEE FIG. 5(b)]

The surface morphology is assumed to be sinusoidal:

$$h_s(x) = h\ \sin\left(2\pi\frac{x}{\lambda}\right), \tag{A1}$$

with h the amplitude and λ the wavelength of the ripple structure. The exchange energy is given in the continuum approximation:

$$f_{ex}(x) = A\left(\frac{\partial\theta}{\partial x}\right)^2, \tag{A2}$$

with A as exchange stiffness. The averaged exchange energy can be calculated as average over one wavelength:

$$\langle f_{ex}\rangle = \frac{1}{\lambda}\int_0^\lambda A\left(\frac{\partial\theta}{\partial x}\right)^2 \mathrm{d}x. \tag{A3}$$

In a first approximation we assume that $h \ll \lambda$ which yields

$$\theta \approx \tan\theta = \frac{\partial h(x)}{\partial x}. \tag{A4}$$

With this approximation the integral can be easily solved yielding

$$\langle f_{ex}\rangle = \frac{A}{2}\left(\frac{2\pi}{\lambda}\right)^2\left(\frac{2\pi h}{\lambda}\right)^2. \tag{A5}$$

This formula is given in the text above and discussed. In the case that the amplitude is not small compared to the wavelength the angle is given by

$$\theta = \arctan\left[2\pi\frac{h}{\lambda}\cos\left(2\pi\frac{x}{\lambda}\right)\right] \tag{A6}$$

and the integral gives

$$\langle f_{ex}\rangle = (2\pi)^3 A\frac{h^2}{\lambda^4}\int_0^{2\pi}\mathrm{d}z\left(\frac{\sin(z)}{1+\left[\frac{2\pi h}{\lambda}\cos(z)\right]^2}\right)^2,$$

$$z = \frac{2\pi x}{\lambda}, \tag{A7}$$

$$\langle f_{ex}\rangle = \frac{A}{2}\left(\frac{2\pi}{\lambda}\right)^2\left(\frac{2\pi h}{\lambda}\right)^2\frac{1}{\sqrt{1+\left(\frac{2\pi h}{\lambda}\right)^2}}. \tag{A8}$$

APPENDIX B: DIPOLAR ENERGY

1. Surface charges [see Fig. 5(a)]

The distribution of the surface charges σ_s [Fig. 5(a)] is given by the scalar product of the magnetization $\vec{M}$ with the surface normal $\vec{n}$,

$$\sigma_s = \mu_0\vec{M}\cdot\vec{n} = \mu_0 M_s\cos(\phi), \tag{B1}$$

with ϕ being the angle between the magnetization and the surface normal. With

$$\tan\left(\frac{\pi}{2}-\phi\right) = -\frac{\partial h_s}{\partial x}, \tag{B2}$$

$$\tan\left(\frac{\pi}{2}-\phi\right) = -2\pi\frac{h}{\lambda}\cos\left(2\pi\frac{x}{\lambda}\right), \tag{B3}$$

and $h \ll \lambda$,

$$\tan\left(\frac{\pi}{2}-\phi\right) \approx \sin\left(\frac{\pi}{2}-\phi\right) = \cos(\phi), \tag{B4}$$

the distribution of surface charges can be written as

$$\sigma_s(x) = -2\pi\mu_0\frac{h}{\lambda}M_s\cos\left(2\pi\frac{x}{\lambda}\right) = -\mu_0 M_{eff}\cos\left(2\pi\frac{x}{\lambda}\right), \tag{B5}$$

with the reduced, effective magnetization

$$M_{eff} = 2\pi\frac{h}{\lambda}M_s. \tag{B6}$$

The stray field energy density can be calculated by means of a Fourier expansion (Ref. 30, p. 124),

$$f_{m,s} = \frac{\mu_0 M_{eff}^2}{2}\sum_k v_k^2\frac{1-\mathrm{e}^{-2\pi|\vec{q}_k|t}}{2\pi|\vec{q}_k|t}. \tag{B7}$$

With the Fourier coefficients of the charge distribution $v_{\pm1} = \frac{1}{2}$ and the respective wave vectors $q_{\pm1} = \pm\frac{1}{\lambda}$ one obtains

$$f_{m,s} = \frac{\mu_0 M_{eff}^2}{4}\frac{1-\mathrm{e}^{-2\pi\frac{t}{\lambda}}}{2\pi\frac{t}{\lambda}}, \tag{B8}$$

and finally

$$f_{m,s} = \frac{\pi\mu_0 M_s^2 h^2}{2t\lambda}\left(1-\mathrm{e}^{-2\pi\frac{t}{\lambda}}\right). \tag{B9}$$

2. Volume charges [see Fig. 5(b)]

Due to the definition of the volume charge density ρ_m

$$\rho_m = \mu_0\vec{\nabla}\cdot\vec{M}, \tag{B10}$$

the only contribution to volume charges originates from a variation of the magnetization in x direction which can be written as

$$M_x = M_s\sqrt{\frac{1}{1+\left[2\pi\frac{h}{\lambda}\cos\left(2\pi\frac{x}{\lambda}\right)\right]^2}}. \tag{B11}$$

The emerging dipolar energy can be calculated from Eq. (11) in Ref. 31 via a Fourier expansion of Eq. (B11). The dominant contribution is given by Fourier coefficients with $j = \pm2$; higher orders can be omitted, smaller orders are zero ($j = 0$ vanishes due to $q_j = 0$). For a surface modulation [Eq. (A1)] of $h = 10$ nm and respective wavelength of $\lambda = 100$ nm this yields

$$f_{m,v} = \frac{\mu_0 M_s^2}{2}\times\ 0.00291\ \times\left(1-\frac{1-\mathrm{e}^{-4\pi\frac{t}{\lambda}}}{4\pi\frac{t}{\lambda}}\right). \tag{B12}$$

For films of thickness $t > 50$ nm a maximum value of $f_{m,v} = 3.58\ \mathrm{kJ/m^3}$ is obtained (see Fig. 6).

*Corresponding author: kai.chen@hzg.de

[1]A. Berger, U. Linke, and H. P. Oepen, Phys. Rev. Lett. **68**, 839 (1992).
[2]J. Chen and J. L. Erskine, Phys. Rev. Lett. **68**, 1212 (1992).
[3]W. Weber, C. H. Back, A. Bischof, C. Würsch, and R. Allenspach, Phys. Rev. Lett. **76**, 1940 (1996).
[4]D. Sekiba, R. Moroni, G. Gonella, F. Buatier de Mongeot, C. Boragno, L. Mattera, and U. Valbusa, Appl. Phys. Lett. **84**, 762 (2004).
[5]R. Moroni, D. Sekiba, F. Buatier de Mongeot, G. Gonella, C. Boragno, L. Mattera, and U. Valbusa, Phys. Rev. Lett. **91**, 167207 (2003).
[6]A. Molle, F. Buatier de Mongeot, C. Boragno, R. Moroni, F. Granone, D. Sekiba, R. Buzio, U. Valbusa, R. Felici, and C. Quiros, Appl. Phys. Lett. **86**, 141906 (2005).
[7]F. Bisio, R. Moroni, F. Buatier de Mongeot, M. Canepa, and L. Mattera, Appl. Phys. Lett. **89**, 052507 (2006).
[8]Q.-f. Zhan, S. Vandezande, and C. V. Haesendonck, Appl. Phys. Lett. **91**, 122510 (2007).
[9]F. Bisio, R. Moroni, F. Buatier de Mongeot, M. Canepa, and L. Mattera, Phys. Rev. Lett. **96**, 057204 (2006).
[10]J. Li, D. Stein, C. McCullan, D. Branton, M. J. Aziz, and J. A. Golovchenko, Nature (London) **412**, 166 (2001).
[11]U. Valbusa, C. Boragno, and F. Buatier de Mongeot, J. Phys.: Condens. Matter **14**, 8153 (2002).
[12]T. K. Chini, D. P. Datta, and S. R. Bhattacharyya, J. Phys.: Condens. Matter **21**, 224004 (2009).
[13]J. Grenzer, A. Biermanns, A. Mücklich, S. A. Grigorian, and U. Pietsch, Phys. Status Solidi A **206**, 1731 (2009).
[14]F. Buatier de Mongeot and U. Valbusa, J. Phys.: Condens. Matter **21**, 224022 (2009).
[15]S. Rusponi, C. Boragno, and U. Valbusa, Phys. Rev. Lett. **78**, 2795 (1997).
[16]S. Rusponi, G. Costantini, C. Boragno, and U. Valbusa, Phys. Rev. Lett. **81**, 2735 (1998).
[17]S. Rusponi, G. Costantini, F. Buatier de Mongeot, C. Boragno, and U. Valbusaa, Appl. Phys. Lett. **75**, 3318 (1999).
[18]M. A. Arranz and J. M. Colino, J. Phys.: Conf. Ser. **200**, 072007 (2010).
[19]M. O. Liedke, B. Liedke, A. Keller, B. Hillebrands, A. Mücklich, S. Facsko, and J. Fassbender, Phys. Rev. B **75**, 220407 (2007).
[20]M. Körner, K. Lenz, M. O. Liedke, T. Strache, A. Mücklich, A. Keller, S. Facsko, and J. Fassbender, Phys. Rev. B **80**, 214401 (2009).
[21]A. Keller, L. Peverini, J. Grenzer, G. J. Kovacs, A. Mücklich, and S. Facsko, Phys. Rev. B **84**, 035423 (2011).
[22]K. V. Sarathlal, D. Kumar, and G. Ajay, Appl. Phys. Lett. **98**, 123111 (2011).
[23]K. Zhang, M. Uhrmacher, H. Hofsäss, and J. Krauser, J. Appl. Phys. **103**, 083507 (2008).
[24]R. Moroni, F. Bisio, F. Buatier de Mongeot, C. Boragno, and L. Mattera, Phys. Rev. B **76**, 214423 (2007).
[25]K. Chen, M. Bubek, R. Frömter, and H. P. Oepen (unpublished).
[26]E. Schlömann, J. Appl. Phys. **41**, 1617 (1970).
[27]R. Arias and D. L. Mills, Phys. Rev. B **59**, 11871 (1999).
[28]N. Mikuszeit, S. Pütter, and H. P. Oepen, J. Magn. Magn. Mater. **268**, 340 (2004).
[29]H. Fujiwara, H. Kadomatsu, and T. Tokunaga, J. Magn. Magn. Mater. **31**, 809 (1983); **34**, 809 (1983).
[30]A. Hubert and R. Schäfer, in *Magnetic Domains* (Springer, New York, 1998), p. 124.
[31]N. Mikuszeit, S. Meckler, R. Wiesendanger, and R. Miranda, Phys. Rev. B **84**, 054404 (2011).